Journal of Hydrology 538 (2016) 339–354

Contents lists available at ScienceDirect

Journal of Hydrology

journal homepage: www.elsevier.com/locate/jhydrol

Infiltration in layered loessial deposits: Revised numerical simulations and recharge assessment

Elad Dafny [a,*], Jirka Šimůnek [b]

[a] National Centre for Engineering in Agriculture, University of Southern Queensland, Toowoomba, QLD 4350, Australia
[b] Department of Environmental Sciences, University of California, Riverside, CA, United States

ARTICLE INFO

Article history:
Received 15 February 2016
Received in revised form 11 April 2016
Accepted 14 April 2016
Available online 21 April 2016

This manuscript was handled by Peter K. Kitanidis, Editor-in-Chief, with the assistance of Juan V. Giraldez, Associate Editor

Keywords:
Infiltration test
Groundwater recharge
Arid vegetation
HYDRUS
Sandy loess
Layered profile

SUMMARY

The objective of this study is to assess recharge rates and their timing under layered loessial deposits at the edge of arid zones. Particularly, this study is focused on the case of the coastal plain of Israel and Gaza. First, results of a large-scale field infiltration test were used to calibrate the van Genuchten parameters of hydraulic properties of the loessial sediments using HYDRUS (2D/3D). Second, optimized soil hydraulic parameters were used by HYDRUS-1D to simulate the water balance of the sandy-loess sediments during a 25-year period (1990–2015) for three environmental conditions: bare soil, and soil with both sparse and dense natural vegetation.

The best inverse parameter optimization run fitted the infiltration test data with the RMSE of 0.27 d (with respect to a moisture front arrival) and R^2 of 96%. The calibrated model indicates that hydraulic conductivities of the two soil horizons, namely sandy loam and sandy clay loam, are 81 cm/d and 17.5 cm/d, respectively. These values are significantly lower than those previously reported, based on numerical simulations, for the same site.

HYDRUS-1D simulation of natural recharge under bare soil resulted in recharge estimates (to the aquifer) in the range of 21–93 mm/yr, with an average recharge of 63 mm/yr. Annual precipitation in the same period varied between 100 and 300 mm/yr, with an average of 185 mm/yr. For semi-stabilized dunes, with 26% of the soil surface covered by local shrub (*Artemisia monosperma*), the mean annual recharge was 28 mm. For the stabilized landscape, with as much as 50% vegetation coverage, it was only 2–3 mm/yr. In other words, loessial sediments can either be a source of significant recharge, or of no recharge at all, depending on the degree of vegetative cover. Additionally, the time lag between specific rainy seasons and corresponding recharge events at a depth of 22 m, increased from 2.5 to 5 years, and to about 20 years, respectively, with an increasing vegetative cover. For this reason, and also likely due to a great depth of loessial sediments, no correlation was found between annual recharge and annual precipitations of the same year or subsequent years. Similarly, no differences were found between summer and winter recharge fluxes. Instead, numerical simulations indicated continuous year-round recharge of the aquifer. We conclude that the layered subsurface acts as a short-term (annual) and long-term (multi-annual) buffer to smooth sudden precipitation/infiltration events. Vegetation conditions can help in predicting long-term recharge rates (as percentage of annual precipitation), which in turn need to be considered when assigning recharge characteristics in regional assessments and models.

1. Introduction

Recharge estimations play an important role in the management and research of groundwater systems. The magnitude and timing of groundwater recharge with respect to the corresponding infiltration events are controlled by climatic and geological factors, as well as the depth to the water table, and have long been of scientific and practical interest (e.g., Wu et al., 1996; Scanlon et al., 2006). Recharge can be estimated by various methods, which should be selected based on the climate zone (arid/humid), expected fluxes, the spatial scale of the aquifer, and the studied time scale (Scanlon et al., 2002a). Such a task should also consider the data availability in terms of soil hydraulic properties and climatic data (e.g., precipitation and evaporation time series).

Physically based models, such as those solving the Richards' equation for water flow in the vadose zone and water balance of surficial sediments, have often been used for estimations of groundwater recharge under various conditions (Wu et al., 1996;

* Corresponding author.

http://dx.doi.org/10.1016/j.jhydrol.2016.04.029
0022-1694/

Scanlon et al., 2002b; Kurtzman and Scanlon, 2011; Leterme et al., 2012; Turkeltaub et al., 2015). These models require the knowledge of soil water retention and unsaturated hydraulic conductivity functions for all soil horizons. Nevertheless, as such knowledge exists (or is measured) only in rare cases, inverse modeling, in which numerical models are calibrated using measured flow-related variables, has gained popularity for estimating the hydraulic functions characterizing the unsaturated zone (Hopmans et al., 2002; Vrugt et al., 2008). Inverse models are then tested by their ability to reproduce independent measurements (Jacques et al., 2002; Ritter et al., 2003; Turkeltaub et al., 2015). Inverse modeling has several important advantages over other methods of estimating soil hydraulic properties. These mainly include (a) the ability to simultaneously estimate both the soil water retention and unsaturated hydraulic conductivity function from a single transient experiment, and (b) the fact that similar numerical models are used both for estimation of soil hydraulic properties (calibration) and for predictive forward modeling (assessment of recharge) (e.g., Hopmans et al., 2002).

Loessial soils are regarded by many as transmissive and rechargeable (Lin and Wei, 2006; Seiler and Gat, 2007; Aish, 2014). Nevertheless under some vegetation and climate conditions they might "*act as an impervious barrier to recharge*" (Weinthal et al., 2005). The objective of this paper is to provide a physically based assessment of recharge rates under loessial soils for arid climate and vegetation. We use the case of the coastal aquifer bounding Israel and the Gaza strip. Large parts of this aquifer are covered by loess and loessial sediments.

The thorough data set collected during a large infiltration test in this area, as reported by Gvirtzman et al. (2008), is first used to quantify the hydraulic conductivities and van Genuchten retention parameters of the loessial sediments of the studied area. Second, calibrated soil hydraulic properties and long-term meteorological data are used to assess the long-term natural recharge to the underlying sandy aquifer. These two modeling stages are sequentially discussed in separate sections. Finally, insights obtained using this recharge model are discussed in relation to previously used models and empirical recharge estimations of the same aquifer. The conclusions obtained in this study for the coastal plain underlying Israel and Gaza Strip are relevant for other phreatic aquifers overlain by a thick, layered unsaturated-zone, especially those within a similar arid climate.

2. Study area

While it is also relevant for other areas on the edge of arid-climate zones, the study focuses on the area covered by sandy loess soils south of the Gaza Strip (Fig. 1). In this area, a relatively thick (>20 m) layer of loessial deposits covers permeable sandy layers of the coastal aquifer (Fig. 1b). The water table is at a depth of about 25–35 m, and the hydraulic gradient is toward the Mediterranean coast, i.e., to the NW.

The term 'loessial deposits' is used here to describe the sandy grain-size loess, according to the Yaalon and Dan (1974) definition, and to distinguish it from silty grain-size loess. The sediments accumulated during the Late Pleistocene period when desert storms brought sands from the northern Sinai Desert to the area (Yaalon and Dan, 1974; Crouvi et al., 2010). Since the distance from the parent material to the accumulation site is relatively short, these wind-blown sediments maintained a fairly coarse-grain composition, contrary to the classic silt-size loess sediments (Crouvi et al., 2010). Nevertheless, the grain size distribution in the loessial sediments is highly variable and depends on the wind speed (Crouvi et al., 2010). During periods of intense winds, active eolian abrasion of the sand grains increased, silt-size sediments were imported, and vice versa. Gradually, a layered sandy loess deposit was accumulated.

The area is dominated by the Mediterranean climate, with dry and hot summers and a rainy season between October and April. The average annual precipitation is about 200 mm/yr. At En Habesor meteorological station (#144872, Israel's Meteorological Service (IMS) database, see location in (Fig. 1a)), an average precipitation of 185 mm/yr was recorded during the last 25 years (1990–2015). The cumulative annual potential evaporation exceeds 1800 mm.

The dominant species in the area is a desert dwarf shrub, *Artemisia monosperma* (Bar Kutiel et al., 2016). It has an important role in the dune stabilization process, and covers up to 16%, 16–36%, and 36–65% of the total area of mobile, semi-stabilized and stabilized dunes, respectively. *A. monosperma* develops a unique root system in response to the accumulating or dispersing sands around it. Similar to other species of dune vegetation, its roots seldom exceed a depth of 3 m, but extend laterally to accommodate any available water from the 'open matrix' in-between neighboring shrubs (Bar Kutiel et al., 2016).

The observed run-off from sandy loess soils in the region is very small (Yair, 1990; Givati and Atzmon, 2009; Eshtawi et al., 2015). For the entire catchment of the ephemeral Besor River, which is covered in large parts by sandy loess sediments, the run-off coefficient for 1985/6–2009/10, defined as % of annual precipitation, was only 1.3% (Givati and Atzmon, 2009). For comparison, the average run-off coefficient over the entire western drainage system of Israel in the same period was 4.4%.

2.1. 2004 Infiltration test

A large trench infiltration test was conducted within the study area in 2004 by Gvirtzman et al. (2008). We only provide here a short description of the infiltration test, its set-up, the measurements made, and the obtained results that are relevant to the current study. Detailed information about the experiment can be found in Gvirtzman et al. (2008).

An elongated trench (3 m wide by 17 m long at the base) was excavated in the loessial section, and its sloping edges were covered by PVC sheets. Four bores (marked 'A' through 'D') were drilled in the vicinity of the trench midline (Fig. 2). Each was equipped with 7–8 TDR probes at different depths, which monitored the temporal changes in the water saturation. The probes were numbered from top to bottom (i.e., probe C2 is deeper than probe C1, etc.). Due to technical issues, only data of 22 sensors was collected, as noted in Fig. 2.

Soil and sediment samples taken from these bores allow for detailed characterization of the profile. Soil moisture, bulk density, porosity, content of fines (<0.075 mm), and other parameters were measured every 2 m (Gvirtzman et al., 2008; Hatzor et al., 2009). Overall, the loessial sediment profile is stratified, with alternating horizons classified as silty sand, clayey sand, and low plasticity clay ('SM', 'SC', and 'CL', respectively) according to the Unified Soil Classification System (USCS). The exact description of the sediment profile, as well as soil physical properties, slightly varied from bore to bore.

In March 2004, following the end of the winter season, the trench was flooded with 1 m of water for 17 days. TDR readings were taken in decreasing frequencies during 20 days of the experiment. The analysis of water content measurements shows that the wetting front propagates below the trench in an 'onion-shape' pattern. The data further indicates that the wetting front reached the lowest probe (C8), located 20 m below the trench base, between

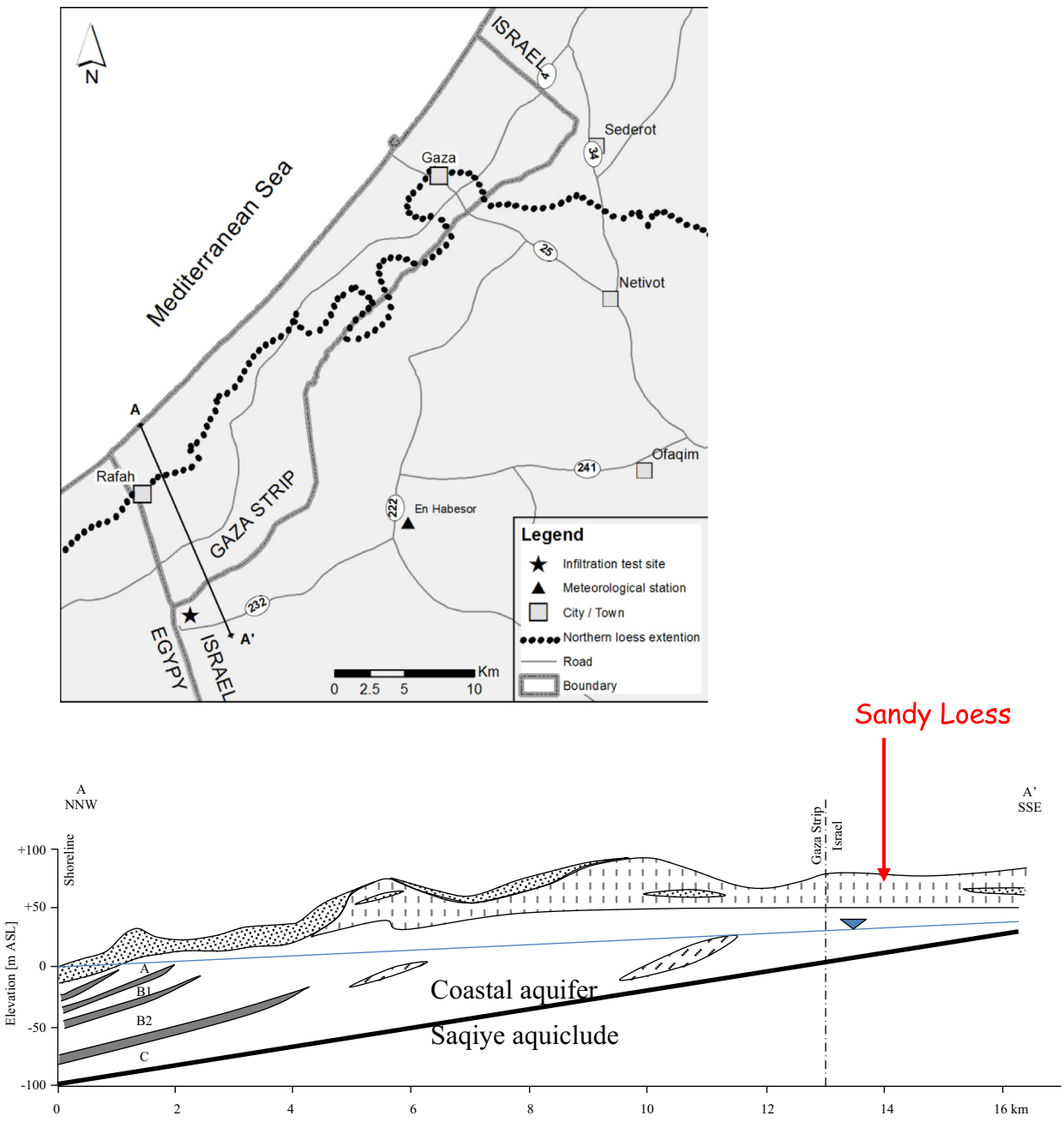

Fig. 1. Location map and geological cross-section (after Tulmatz, 1977).

days 17 and 20 (i.e., at 8:00 a.m. on the 17th day, the sensor was still dry, and by 8:00 a.m. on the 20th day, it was already wet). The overall water volume used to fill the trench in this experiment was 1400 m^3. Inevitably, a small portion of water, which filled the trench, directly evaporated.

A second experiment was carried out about three months later in July 2004. For this experiment, the trench was lengthened to 48 m. The sides of the trench were re-sheeted with PVC sheets. The trench was then flooded with 1.25 m of water for 25 days. TDR readings were taken less and less frequently during the 4th, 7th, 10th and 14th days of the experiment. The wetting front propagation during the second experiment was noted to be substantially faster than its propagation during the first experiment, though the results were not reported in the paper. The overall water usage in this experiment was 10,300 m^3.

3. Inverse calibration of the first infiltration test

The results of the first infiltration test served to calibrate the hydraulic properties of the loessial sediments. The high uncertainties and generally less meticulous data for the second infiltration test prevented it from serving as a validation test. Among other issues, the water use (and percolation rate) in the second infiltration experiment was substantially higher than expected. Had the infiltration rate been the same as in the first test, the water use would have been 5813 m^3 (1400 $m^3 \times (25\ d/17\ d) \times (48\ m/17\ m)$). Furthermore, had the infiltration rate increased due to the higher head in the trench, the water use would have been 7266 m^3 ($5813 \times 1.25/1.0$). However, the reported water use was 41–71% higher than expected. This difference cannot be caused by variations in the initial conditions at the onset of the

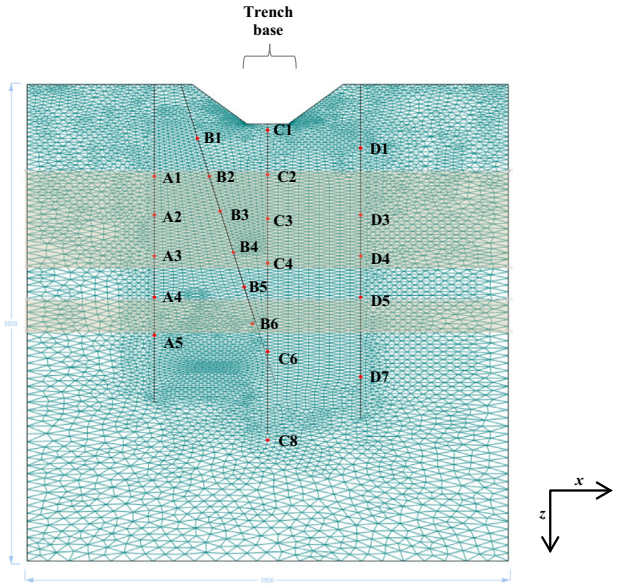

Fig. 2. 2D domain showing the bores (black lines), finite element mesh (blue lines), and observation points (red). The diagram is 30 m high and 35 m wide. (For interpretation of the references to color in this figure legend, the reader is referred to the web version of this article.)

two experiments (as also demonstrated by our numerical results, simulations not included here). Direct evaporation from the trench, in the order of 7.6 mm/d during July (see Section 4.1.2) could explain only a fraction of the difference (only 47 m^3). We hypothesize (partly based on a comparison of photos included in Gvirtzman et al. (2008) and Hatzor et al. (2009)) that the trench cover was less durable (hence less effective) during the second test, thus increasing the effective percolation area. Alternatively, there may have been technical issues with the water level or water use metering.

3.1. Methods

3.1.1. Model settings

Numerical simulations of the infiltration experiment were conducted using version 2.03.0450 of the HYDRUS (2D/3D) code (Šimůnek et al., 2008). The code solves the two-dimensional (2D) form of the Richards' equation while allowing for time-variable boundary conditions. In order for the results to be comparable to the previous study, a 2D domain resembling the one described by Gvirtzman et al. (2008) was considered in numerical simulations. The domain was set perpendicular to the flooded trench, assuming that a 3D flow pattern can be approximated using the flow field in the 2D x–z plane (where x and z are the horizontal and vertical coordinates). This approximation seems to be justified, as the length of the trench (17 m, in the y direction) is significantly longer than its width (3 m; in the x direction). Regardless, the 2D domain is adequate to simulate the flow field in the central part of the trench, and it represents recharge through a one length unit.

The 2D transport domain is 35 m wide and 30 m deep, with a 2.5 m-deep trench located in the middle of its upper surface (Fig. 2). The total area of the transport domain is 1032.5 m^2. The profile is comprised of two soil units that form a sequence of five horizons (Table 1). Due to the heterogeneity between different bores, no attempt was made to further sub-divide the subsurface into distinct units. The locations of TDR probes were explicitly introduced into the domain prior to generating the unstructured finite element grid. The average cell size for the entire transport domain was set to 20 cm, with point refinements (of 5 cm) at both edges of the trench bottom and coarsening (of 50 cm) along the bottom part of the domain. The final mesh consists of 11,783 finite elements, substantially less than the 24,174 elements of the structured grid used by Gvirtzman et al. (2008) in their model.

Table 1
Vertical discretization of the 2D domain.

Horizon	Elevation [m]	Soil classification	No. of observation points
1	30–24.5	Sandy loam	3
2	24.5–18.5	Sandy clay loam	11
3	18.5–16.5	Sandy loam	3
4	16.5–14.5	Sandy clay loam	1
5	14.5–0.0	Sandy loam	4

The trench base (3 m wide) was set as a *variable head boundary* (HYDRUS specific technical terms are in italics) to represent ponding. The trench was assumed to fill-up within 6 h to a final pressure head of 100 cm. Following the end of the infiltration test, it drained at a rate of the effective saturated hydraulic conductivity, i.e., for about three days. The bottom of the domain was assumed to be under a unit gradient condition and was set accordingly as a *free drainage boundary*, as it is located far above the water table. The left- and right-hand sides, as well as the top of the domain (except for the trench topography), were assumed to be no-flow boundaries.

The initial pressure head profile was set according to measured moisture contents of the profile using the soil's saturation-pressure functions. Overall, the pressure head alternates between −490 cm and −410 cm, for the more permeable and less permeable horizons, respectively. Note that higher values of the pressure head (−300 cm) were used in the previous model (Gvirtzman et al., 2008) throughout the entire profile.

3.1.2. Calibration strategy

The soil hydraulic properties were calibrated in a series of inverse simulations for the first infiltration test (days 0–21). The van Genuchten soil hydraulic parameters of both soil layers were inversely optimized by the HYDRUS-2D software using the internal Marquardt–Levenberg-type (Marquardt, 1963) parameter optimization algorithm. For the inverse calibration, time series of water contents at each monitoring point (sensor) were reconstructed based on the available data from the first infiltration experiment. These time series included the timing of the first reading when the probe was found to be wet and the last reading when it was still dry. Each time series thus contained, at least, three observations. The initial, low water content, which was assumed to be constant until the arrival of the moisture front, was used initially (t = 0 d) and at the last time that the data logging suggested that the sensor was dry. A relatively high water content (90% of the saturated water content of a particular soil) was used at the next data logging, after the arrival of the wetting front. For example, for the C8 sensor, θ = 0.054 was set at t = 0 and 16.8 d and θ = 0.33 was set at t = 19.8 d. For three probes in the uppermost part of the profile (B1, C1, and C2), the data included discrete readings of water contents 4–5 times during the experiment. These sensors showed a gradual transition from dry (θ = 0.05) to wet (θ = 0.40) conditions, over 5 h to 4 days.

Additionally, the net cumulative volume of water that infiltrated to the subsurface during the experiment (total cumulative influx minus evaporation) was used to constrain the solution. The water volume used in the experiment was first divided by the length of the trench, and then potential evaporation during the experimental period (Section 4.1.2) was subtracted to give cumulative infiltration flux (81.6 m^3/m length), which was used during inverse optimization.

The inverse parameter estimation was conducted by minimizing the objective function (Šimůnek et al., 2009):

$$\varphi = v_\theta \sum_{i=1}^{n} w_i [\theta_{obs}(t_i) - \theta_{sim}(t_i)]^2 + v_{cf} w_{cf} [cf_{obs} - cf_{sim}]^2 \quad (1)$$

where n is the number of water content observations, θ_{obs} and θ_{sim} are measured and simulated volumetric water contents at times t_i, w_i is the weight for individual observations, w_{cf} is the weight for the cumulative infiltration, and cf_{obs} and cf_{sim} are measured and simulated cumulative infiltrations at the end of the experiment. Due to relatively large uncertainties involved, the observations weights (w_i and w_{cf}) were set to 0.1, to allow for a wider confidence range. v_θ and v_{cf} are the model-assigned weighting coefficients, which minimize differences in weighting between the water content data set and the cumulative flux data set.

The inverse calibration was carried out to estimate at once six soil hydraulic parameters (three for each soil unit): the saturated hydraulic conductivity K_s, and the α and n parameters (which control the shape of the retention curve). The residual and saturated water contents (θ_r and θ_s, respectively) were set to representative values obtained in the field and lab (Hatzor et al., 2009) (Table 2). The pore connectivity and tortuosity factor l, which showed to be unimportant and/or insensitive in numerical experiments (e.g., Wang et al., 2003; Turkeltaub et al., 2015), was fixed at 0.5 for both soil units (Mualem, 1976).

Uniqueness and stability of the inverse solution were tested by repeatedly solving the inverse problem using six different combinations of the observations while setting various initial estimates for the calibrated parameters. The list of optimized parameters and different combinations of the observations is given in Table 4, which also gives the final optimized values (discussed below).

3.2. Results

The simulated instantaneous infiltration rate through the trench floor at the beginning of the first test was very high (13.2 mm/min). The infiltration rates exponentially fell until stabilizing at a much lower level of about 0.9 mm/min, which is equivalent to 3.8 m^3/m length/d. The cumulative infiltration during the first test was 81.6 m^3/m length. Integration of the simulated infiltration rate during the first flood over the 17 m trench resulted in a total of 1387 m^3, with a perfect match of the measured influx (accounting for the calculated direct evaporation of 13 m^3). During this period, no recharge occurred under the experiment site, i.e., almost all infiltrated water remained (temporarily) in the unsaturated zone.

Table 2
Fixed (not calibrated) soil hydraulic parameters.

Soil unit	θ_r [ ]	θ_s [ ]	l [ ]
Sandy loam	0.035	0.38	0.5
Sandy clay loam	0.085	0.36	0.5

The simulated wetting front propagation for the first infiltration test satisfactorily matched the conceptualized (Gvirtzman et al., 2008) wetting front propagation, as demonstrated in Fig. 3. Though Fig. 3a may suggest some mismatch in the early stages of the simulation, careful examination of the first arrival times shows that the simulated results matched at least 3 out of 6 early observations of saturation (i.e., C1, C3, D1). Using the considered conceptual setup, it was not possible to further reduce discrepancies between measured and simulated arrivals of the wetting front at the other three observation points (B1, B2, and C2), as well as at five other points (Fig. 4). Similar discrepancies were described in earlier studies (Wierenga et al., 1991; Zou et al., 2001; Gvirtzman et al., 2008; Turkeltaub et al., 2015) and were attributed to the inherent heterogeneity of the natural soil material, including the spatial variability of hydraulic conductivities and the uncertain thickness of different soil horizons. Thus, a better fit for each and every measurement point was not expected nor pursued. Regardless, a very good match can be seen from day 13 onward (Fig. 3b and c).

It should be noted that all simulated wetting front arrivals at bore B were earlier than observed. For that reason, we conducted 6 runs using and/or excluding various parts of the dataset. For example, information collected in bore B was excluded in run #2, and information collected in the top 10 m of the profile was excluded in run #6. Table 3 indicates that all calibration runs produced the same narrow range of hydraulic conductivities for both soil units, regardless of what observation sets were used. Table 4 summarizes the statistical results of the runs. Excluding bore B observations did not change the calibration results (compare runs #1 and #2 in Table 3), although it slightly improved the statistical fit. This means that it is unlikely that the calibration is biased by data from one or more bores (particularly bore B) or from the depth at which they were taken.

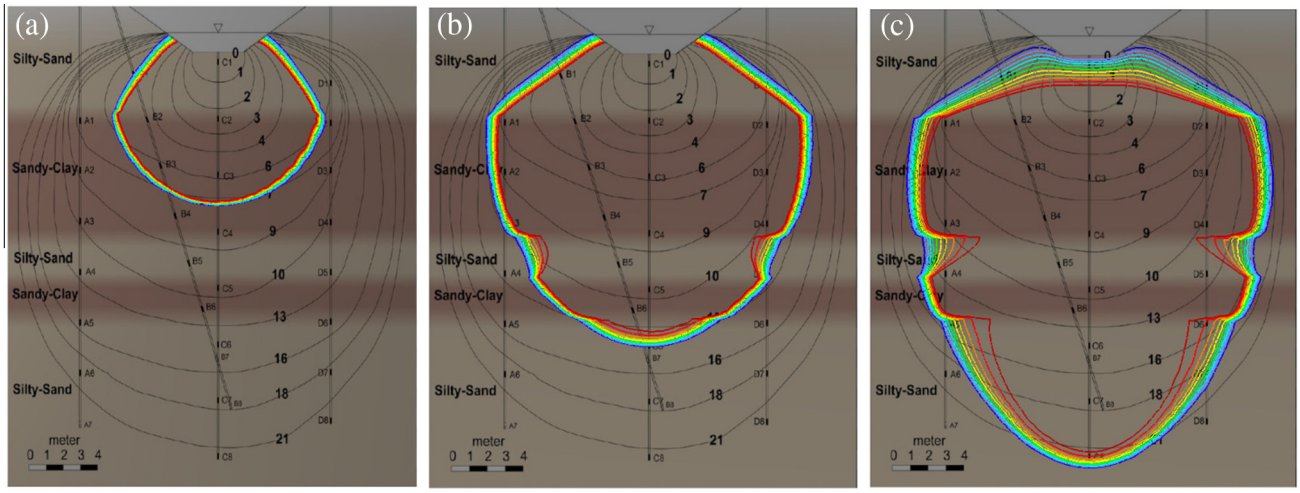

Fig. 3. Simulated (colored) and conceptualized (background) water content profiles at three times during the first infiltration experiment: (a) day 4, (b) day 13, and (c) day 21. Each diagram is 30 m high and 35 m wide. The colored contours depict water content of 19% (blue) and 29% (red). Background image is Fig. 6 of Gvirtzman et al. (2008). (For interpretation of the references to color in this figure legend, the reader is referred to the web version of this article.)

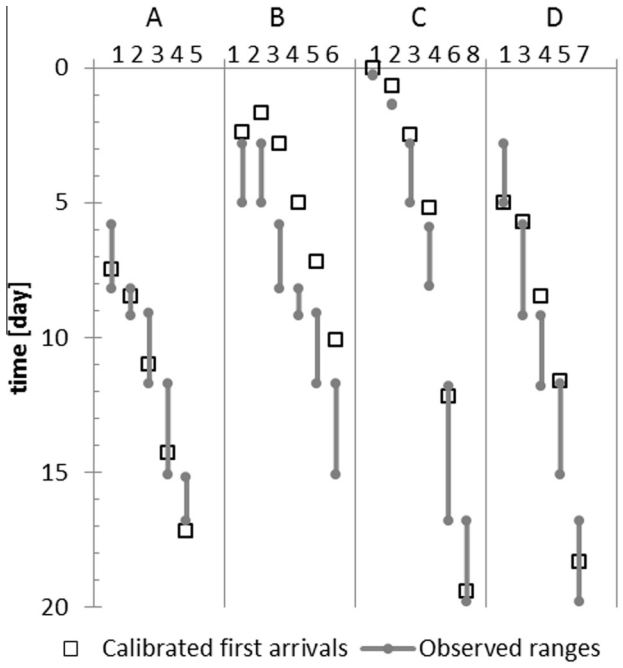

Fig. 4. Simulated and observed (ranges) arrival times of the wetting front at various probes (bores (A–D and probe numbers are shown in the upper row).

Based on these inverse optimization runs, the hydraulic conductivities of the two soil units were set to $K_1 = 80.2$ cm/d and $K_2 = 17.3$ cm/d. These calibrated values are substantially lower than those previously proposed based on numerical simulations (i.e., 1103 cm/d and 525 cm/d, respectively, Gvirtzman et al. (2008)). The previous, higher values would generally characterize sandy soils, rather than loamy soils (Radcliffe, 2002). For example, calibrated hydraulic conductivities for five sandy soils at a nearby site range between 1069 and 1756 cm/d, while that of a sandy loam soil was only 41 cm/d (Turkeltaub et al., 2015).

3.3. Soil classification

The calibrated saturated hydraulic conductivities for the two soil units were $K_1 = 80.2$ cm/d and $K_2 = 17.3$ cm/d. These values are in the range of conductivity values for 'sandy loam' and 'sandy clay loam' soils, respectively (Radcliffe and Šimůnek, 2010). A further analysis of the grain-size distribution using the USDA soil textural triangle (Hillel, 2004) rather than the USCS', justifies the above soil classifications. Soil samples taken from the high-conductivity layers contain 16–38% fines (i.e., grain smaller than 0.075 mm, as reported by Gvirtzman et al., 2008), with a median of 31% fines. Therefore, the proportion of sands (including the fine sands category) in this soil unit is in excess of 70% and can thus be classified as either sandy loam or sandy clay loam. Similarly, the low-conductivity layers containing 57–68% fines, with a median of 60% fines, can be classified as silt loam, loam, clay loam, or sandy clay loam. Due to a lack of a further analysis of grain-size distribution, besides a general knowledge of the relatively low content of clay in the area's loess (Eshtawi et al., 2015), the final classification of the two soils was made based on the measured and calibrated van Genuchten parameters. The high sand content layer was denoted 'sandy loam' and the low sand content unit was denoted 'sandy clay loam' (Tables 1 and 2). It should be noted that we found the use of the USCS term 'low plasticity clay' for the latter soil unit misleading.

The behavior of the entire system can be perceived as slightly anisotropic, though not due to an initial explicit parameterization. Simple calculations (Fetter, 2001) for the upper 22 m section give an effective vertical hydraulic conductivity ($K_{v,eff}$) of about 35 cm/d and an effective horizontal conductivity ($K_{h,eff}$) of 62 cm/d. The anisotropy is thus about 2 (i.e., the effective horizontal hydraulic conductivity is twice as large as the effective vertical one), merely due to soil layering. Similar low anisotropy values in sandy loam soils, especially following long periods of no-tillage, were described in previous studies (e.g., Petersen et al., 2008). The low implicit anisotropy of the loessial sediments is in contrast with the much higher, conventional, 1:10 explicit anisotropy of the sandy layers of the Israeli coastal aquifer (Amir et al., 2013).

Table 4
'Goodness of calibration' statistics for different inverse runs.

Run	Observation sets	Observation nodes	Min error [d]	Max error [d]	RMSE [d]	R^2[a] (%)
1	All bores	22	0	3.2	1.14	91
2	All bores except B	16	0	0.7	0.27	96
3	Bores A and D	10	0	1.2	0.60	92
4	Bores B and C	12	0	3	1.43	93
5	Only probes in top 10 m	10	0	3	1.06	71
6	Only probes below top 10 m	12	0	1.5	0.95	90

[a] R^2 varies for each run, depending on which data were considered in calibration.

4. Natural recharge simulations

At the second stage, HYDRUS-1D (Šimůnek et al., 2009) was used to assess natural recharge over a 25-year period through loessial sediments similar to those found at the infiltration test site. These recharge simulations aim to explore the overall water

Table 3
Calibrated van Genuchten (1980) parameters and their 95% confidence intervals for two soil materials (subscripts 1 and 2) and different inverse runs.

Run	Observation sets	K_1 [cm/d]	n_1 [–]	α_1 [1/cm]	K_2 [cm/d]	n_2 [–]	α_2 [1/cm]
1	All bores	80.13 (79.98–80.27)	2.68 (2.68)	0.0079 (0.0079)	17.35 (17.35)	3.06 (3.06)	0.0058 (0.0058)
2	All bores except B	81.34 (80.27–81.40)	2.72 (2.70–2.74)	0.0078 (0.00779–0.00785)	17.14 (17.13–17.15)	2.82 (2.78–2.86)	0.0070 (0.0070)
3	Bores A and D	80.11 (80.11)	2.68 (2.41–2.95)	0.0079 (0.0072–0.0086)	17.35 (17.35)	3.05 (3.05)	0.0058 (0.0049–0.0067)
4	Bores B and C	81.34 (81.23–81.45)	2.72 (2.71–2.73)	0.0078 (0.0077–0.0078)	17.14 (17.14)	2.82 (2.77–2.86)	0.0070 (0.0066–0.0073)
5	Only probes in top 10 m	80.38 (79.99–80.78)	2.73 (2.73)	0.0078 (0.0078)	17.46 (17.20–17.73)	2.84 (2.84)	0.0068 (0.0055–0.0082)
6	Only probes below top 10 m	81.34 (79.93–82.75)	2.72 (2.57–2.88)	0.0078 (0.0076–0.0080)	17.14 (17.14)	2.82 (2.82)	0.0070 (0.0058–0.0082)
Statistics: Average range		80.77 (79.93–82.75)	2.71 (2.41–2.95)	0.0078 (0.0072–0.0086)	17.26 (17.13–17.73)	2.90 (2.77–3.06)	0.0066 (0.0049–0.0082)

balance of the vadose zone, including its main six components – precipitation (rainfall), evaporation, infiltration, runoff, recharge, and the change in soil water storage. The simulations have been carried out for three scenarios involving three different natural settings, namely, bare soil, sparse vegetation upon semi-stabilized dunes, and denser vegetation upon a stabilized landscape. These three settings represent successive steps in the stabilization of a typical loessial landscape at the fringe between the arid Sinai Peninsula and the Mediterranean climate (Bar Kutiel et al., 2016).

4.1. Methods

4.1.1. Model settings

The sediment profile was considered to be 22 m deep, i.e., to match the maximal depth from which soil data was obtained during the infiltration test. It was discretized using 150 finite elements of varying sizes, from 0.29 cm at the top to 29 cm at the bottom of the profile. The sediment profile had the same layout (depths of soil horizons and their hydraulic parameters) as the 2D model of the infiltration site. Eight additional realizations, with a combination of ±10% of hydraulic conductivities for the two soil units, were also run to test the sensitivity of the results. The ±10% variations exceed the 95% confidence intervals for the hydraulic conductivities of the two soil materials, as obtained in the simulations of the infiltration test (±3% for both). Five observation points that enabled the recording of changing pressure heads, water fluxes, and water contents, were defined at the bottom of every soil horizon.

An *atmospheric boundary condition with surface run-off* was assigned to the upper boundary of the transport domain. This boundary condition allows water to infiltrate, evaporate, and/or discharge as surface run-off depending on prescribed precipitation and potential evaporation rates, as well as on the transient soil conditions (moisture). This boundary condition requires the setting of a single empirical parameter, *hCritA*, which determines the minimum allowed pressure head at the soil surface and separates the first and second stage of evaporation. This parameter was assigned a value of −15,000 cm, which is the default value for relatively coarse-grain soils. Multiple runs with lower values, down to −100,000 cm, produced similar results, indicating that modeling results (in the scope of this paper) are not sensitive to variation in *hCritA*. Precipitation and potential evaporation fluxes are described in the following section. The bottom of the sediment profile was assumed to be under a unit gradient condition, and was set accordingly as a *free drainage boundary* because it is still located far above the water table.

The initial conditions for each of the three simulations were obtained following initial runs with the proper vegetation parameters (Section 4.1.3) and 100 repetitions of the 1989/90 meteorological conditions (Section 4.1.2).

4.1.2. Meteorological data and temporal variables

Two meteorological data sets were obtained from the Israeli Meteorological Service (IMS) website in order to represent local conditions in the simulations of the recharge to the aquifer: (1) time series of daily precipitation from 1/10/1990 until 30/9/2014; and (2) time series of daily pan evaporation from 1/10/1990 to 31/12/1999 (no evaporation data were recorded thereafter). Both sets were recorded at the En Habesor station, which is located in the middle of the study area (Fig. 1).

The precipitation time series (Fig. 5a) was comprised of daily values. To approximate higher intensity rainfalls than the daily values that occur in this area, each time record was further divided into a short period (0.1 d), which was given the entire daily precipitation volume and a longer period (0.9 d) without precipitation. For example, a day with a total precipitation of 12 mm would be divided into a 2.4-h period with 120 mm/d precipitation (120 mm/d* 0.1 d = 12 mm) and a 21.6-h period without precipitation. This is a more realistic conceptualization of the local weather patterns, and in turn, resulted in higher and more realistic rain intensities (for the example above it is 5 mm/h vs. 0.5 mm/h, respectively) and run-off.

The pan evaporation dataset included some records (about 15% of the records each year) that were obtained over a period of several days rather than for every single day. For this reason, the obtained data could not be used directly. Rather, a synthetic annual time series was prepared based on the collected data, as follows. Overall, daily evaporation varied between about 1 and 9 mm/day, without any significant differences between years (Fig. 5b). The lowest values were recorded each year during January and the highest values during July. Accordingly, a sinusoidal function was fitted to observed daily evaporation values:

$$EV_d = \sin\left(\pi * \left(\frac{DOY}{365}\right)\right) * EV_{fluc} + EV_{min} \quad (2)$$

where EV_d is daily pan evaporation, DOY is the day within the calendar year (e.g., 1st of October of each year is DOY = 273), EV_{min} is minimal daily evaporation on January 1st, set to be 0.8 mm/d, and EV_{fluc} is the amplitude, at which the daily evaporation fluctuates throughout the year. EV_{fluc} was optimized to fit the average annual potential evaporation during a hydrological year (1850 mm/yr) and was found to be 6.8 mm/d. Overall, there is a good match between the synthetic evaporation series, the daily measured values, and a 7-day running average (Fig. 5b).

Finally, a time series of rainfall and potential (pan) evaporation for 25 years (October 1990 to May 2015) was reconstructed by repeating the existing records; this served as input to the 1D model.

4.1.3. Natural vegetation parameterization

The natural vegetation of *A. monosperma* was represented in the numerical model by a set of simplifications. First, its *soil cover fraction* (SCF) was assumed to be 26% for semi-stabilized dunes and 50% for stabilized landscape, that is, an average of reported values (Bar Kutiel et al., 2016). Its *leaf area index* (LAI) index was accordingly calculated using Eq. (3) (Ritchie, 1972):

$$\mathrm{LAI} = -\frac{1}{\alpha} * \ln(1 - \mathrm{SCF}) \quad (3)$$

where α is an empirical parameter, representing the radiation extinction by the canopy, which equals a default value of 0.463. An LAI of 0.65 and 1.49 were calculated for semi-stabilized and stabilized landscapes, respectively.

Second, the vertical root distribution was simplified as follows. For both vegetation settings, no roots were set in the 0–5 cm depth interval, and linear growth was assumed in the 5–30 cm interval. For the semi-stabilized scheme, a logarithmic decrease in root density toward 0 was set in the 30–100 cm depth interval. For the stabilized landscape, vegetation was assumed to be more acclimatized, with a maximal density in the 30–50 cm and a logarithmic decrease toward 0 in the 50–250 cm interval (Fig. 6).

Finally, for the root water uptake, we used the Feddes model (Feddes et al., 1978) with the default HYDRUS values for wheat (Wesseling et al., 1991). The latter was used in light of a lack of more appropriate values in the literature. Importantly, the wilting point pressure head was $P3$ = −16,000 cm and the anaerobiosis point pressure head was $P0$ = 0, i.e. extraction of water from the soil can occur, virtually, under any saturation level.

To verify that the pre-set rooting depth and parameters of the water stress response function in the Feddes model do not have a substantial effect on the results, we ran additional simulations for the semi-stabilized scenario, with a higher (less negative) and

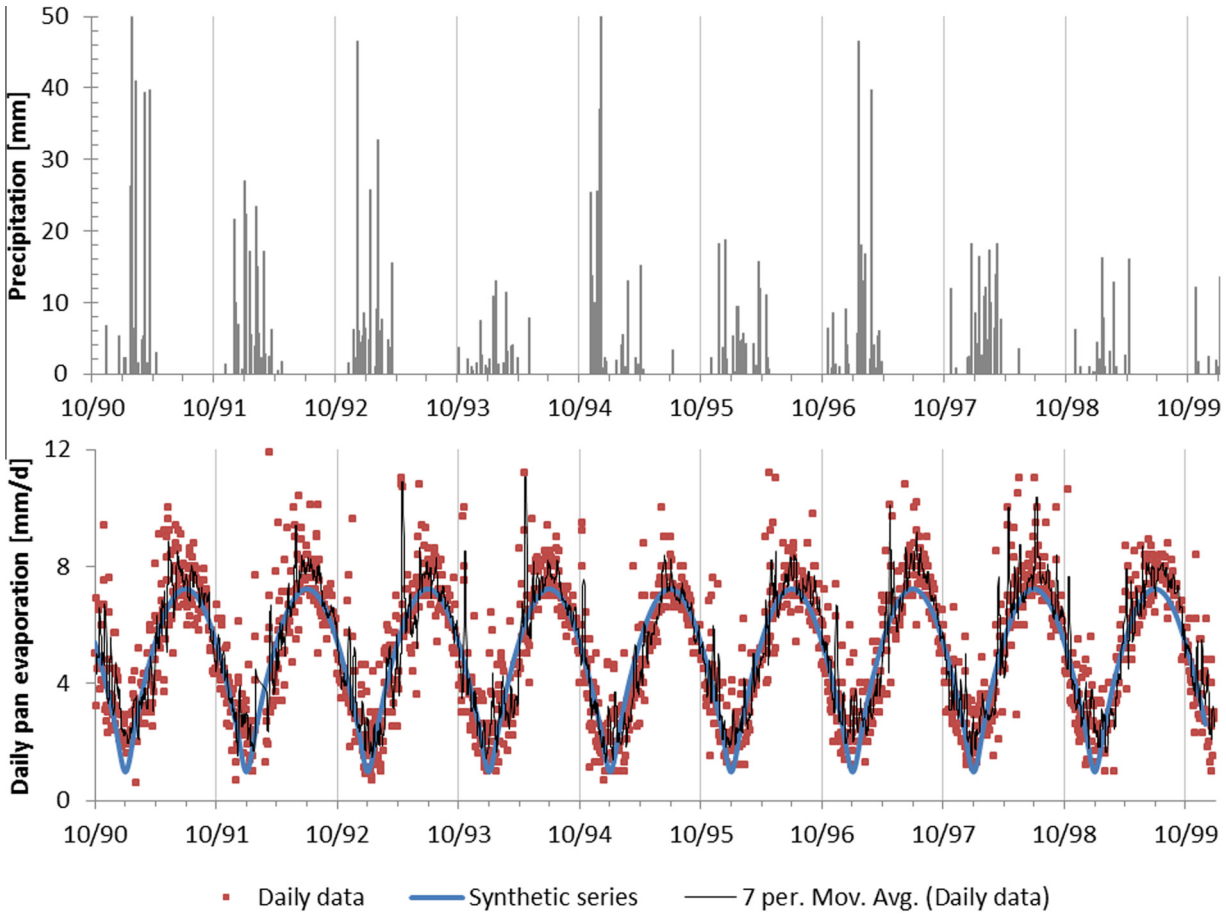

Fig. 5. Daily precipitation (a) and daily evaporation (b) at the En Habesor meteorological station for years 1990/91–1998/99.

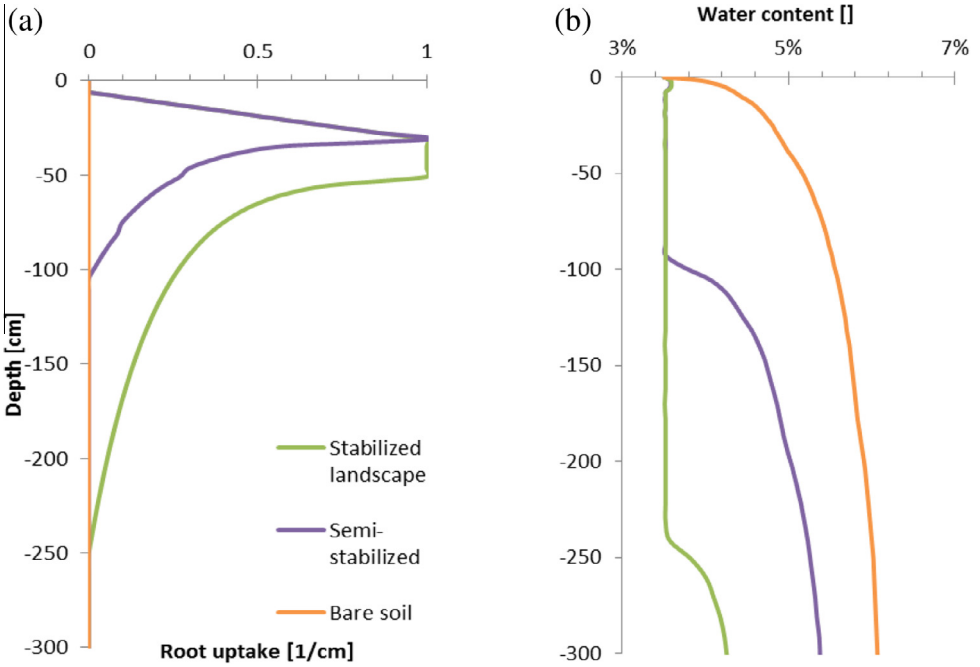

Fig. 6. Root distribution (a) and initial water content (b) in the upper 3 m of the soil for three scenarios. (For interpretation of the references to color in this figure legend, the reader is referred to the web version of this article.)

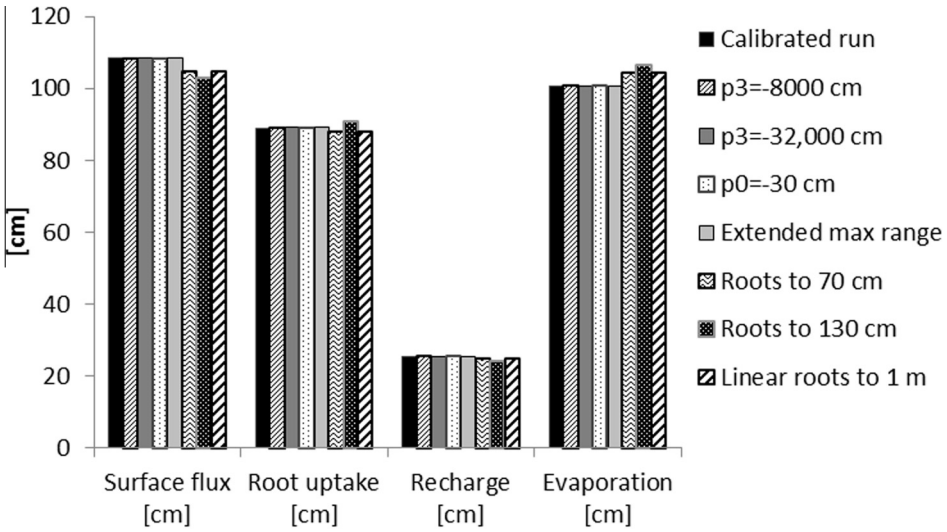

Fig. 7. Changes in cumulative surface flux, root uptake, recharge and evaporation for the amended semi-vegetated simulations during the 1999/2000–2008/9 period. Index lists the changes made, see text for further explanation.

Table 5
Simulated water balance components for a 25-year period (mm and % of precipitation).

	Bare soil	Semi-stabilized	Stabilized landscape
Precipitation (P)	5328 (100%)	5328 (100%)	5328 (100%)
Actual Evaporation (AE)	3624 (68%)	2498 (47%)	2219 (42%)
Runoff (RO)	4 (0.1%)	5 (0.1%)	4 (0.1%)
Net Infiltration (I) (I = P − AE − RO)	1700 (31.9%)	2825 (52.9%)	3105 (57.9%)
Transpiration (T)	0 (0%)	2170 (40.7%)	2961 (55.6%)
Change in storage in the root zone (M1)	+14 (0.3%)	+5 (0%)	+6 (0%)
Deep drainage (DD) (DD = P − AE − RO − T − M1)	1686 (31.6%)	650 (12.2%)	138 (2.6%)
Change in storage below the root zone (M2)	+162 (3%)	+6 (0.1%)	+24 (0.4%)
Recharge (R) (R = DD − M2 + ER)	1544 (29%)	683 (13%)	63 (1%)
Simulated mass balance error (an error of the numerical solution) (ER)	−20 (−0.3%)	−39 (−0.7%)	+51 (0.9%)

a lower wilting point pressure head, $P3 = -8000$ cm and $P3 = -32{,}000$ cm, respectively), a lower anaerobiosis point pressure head ($P0 = -30$ cm), an extended range at which roots can extract water at the maximum rates (by doubling $P2H = -1000$ cm and $P2L = -1800$ cm), shallower and deeper root zones (70 and 130 cm, respectively), and a linear decrease in root density in the 30–100 cm interval. All in all, these runs demonstrate that the results are virtually insensitive to the selected parameters (Fig. 7). For example, recharge rates (P/R) during the 1999/2000 – 2008/9 period were 12.2% for all the simulations testing Feddes parameters, and slightly lower (11.5–12.0%) for the three simulations with various rooting schemes.

4.1.4. Analysis of simulation results

The water balance was calculated for the root zone and the sediments below the root zone. Deep drainage (flux at the bottom of the root zone), which is not included among the reported HYDRUS results, was obtained by subtracting actual transpiration and the change of storage in the root zone from net infiltration. Bottom flux was serving as a proxy to recharge. Cumulative precipitation, evapotranspiration, net infiltration, soil moisture changes, and recharge for the 25-year simulation were divided into annual values. The annual values were tested for their probability distribution using the quantile method (Helsel and Hirsch, 2002, p. 27). The temporal variability of annual precipitation, annual deep drainage, and annual recharge were statistically analyzed. Then, annual values were cross-correlated to demarcate or refute possible interrelations.

To detect the wetting front propagation in the sediment profile, simulated vertical fluxes as recorded at the bottom of each soil horizon were used. The wetting front was assumed to propagate downward following seasonal rains, with a decreasing amplitude and an increasing time-lag (Wu et al., 1996). The merging of a few annual peaks was expected to occur at larger depths, especially in scenarios with low annual deep drainage. Fortunately, the data record contained two rainy years (1994/1995 and 2004/5) with precipitation of +50% above average. These two years produced fairly high net infiltration and deep drainage. The resulted flux peaks could be traced down to the depth of the simulated profile and served to delineate the precipitation–recharge time lag. Next,

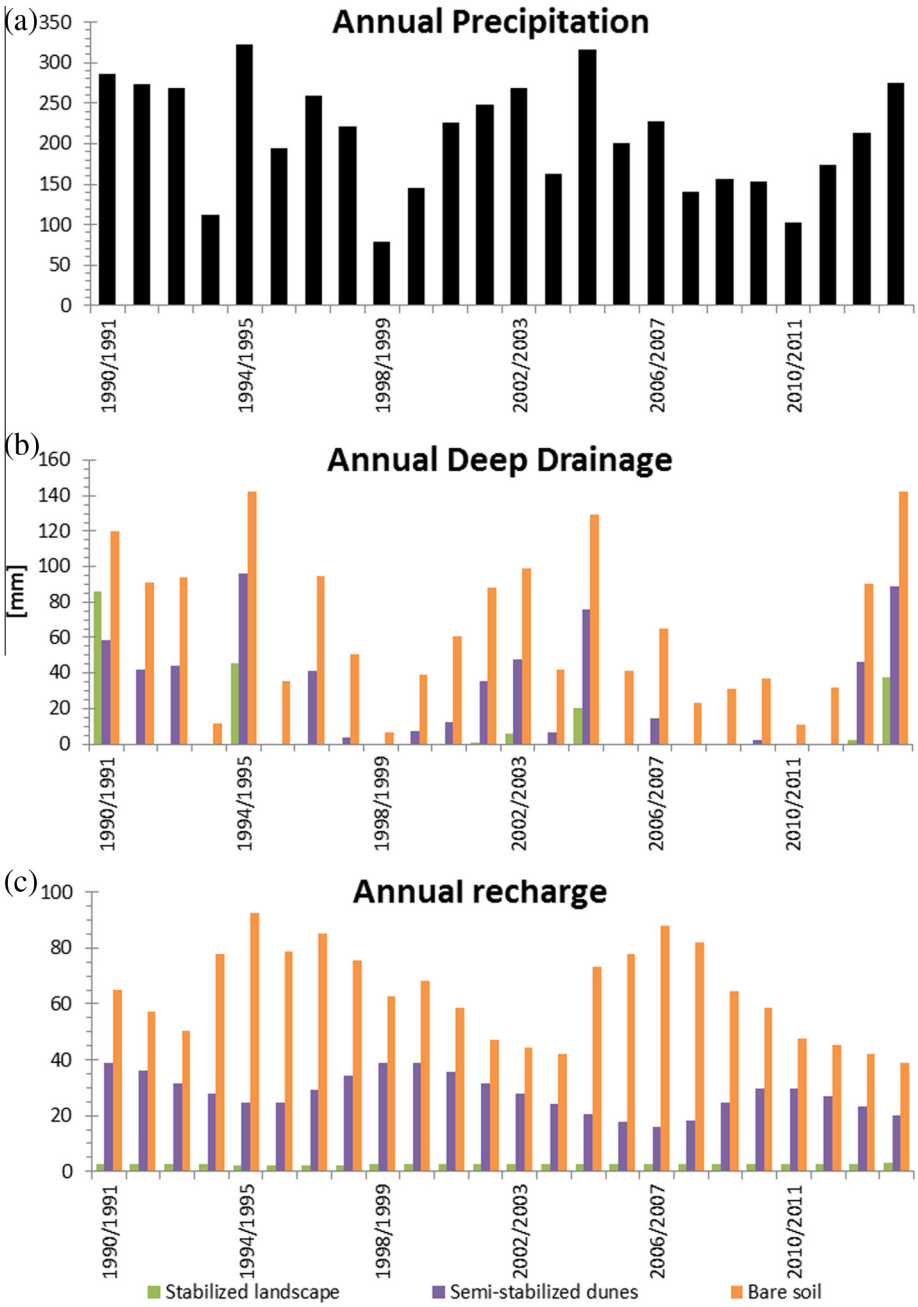

Fig. 8. Simulated annual precipitation (a), deep drainage (b), and recharge (c) for the three scenarios. (For interpretation of the references to color in this figure legend, the reader is referred to the web version of this article.)

a few other peaks and lows in the flux time-series were correlated to rain events with the same time lags. For the stabilized landscape scenario this was conducted only for the first peak, due to a high detected time lag.

4.2. Results

The following section discusses water balances and different fluxes for the three evaluated scenarios. For consistency, all length variables reported in this section are in mm.

4.2.1. Water balance

Total recharge and five other components of the water balance, as simulated for the 25-year period and the three scenarios, are summarized in Table 5. Net infiltration (I) is the result of subtracting actual evaporation (AE) and runoff (RO) from precipitation (P) at the same time interval. Deep drainage (D), which is the flux at the bottom of the root zone, is obtained by subtracting the actual transpiration (T) and the change of storage in the root zone (M1) from net infiltration. And finally, recharge (R) is the result of further subtracting changes in soil storage below the root zone (M2) from deep drainage. One should note that simulated mass balance errors are kept very low (less than 1% of the overall water budget).

Annual time series of precipitation, deep drainage, and recharge for the three scenarios are shown in Fig. 8. Simulated annual precipitation perfectly matched observed precipitation. Statistical analysis shows, with high confidence, that annual precipitation and recharge are normally distributed (i.e., the null hypothesis could not be rejected). Run-off was rather constant and small in

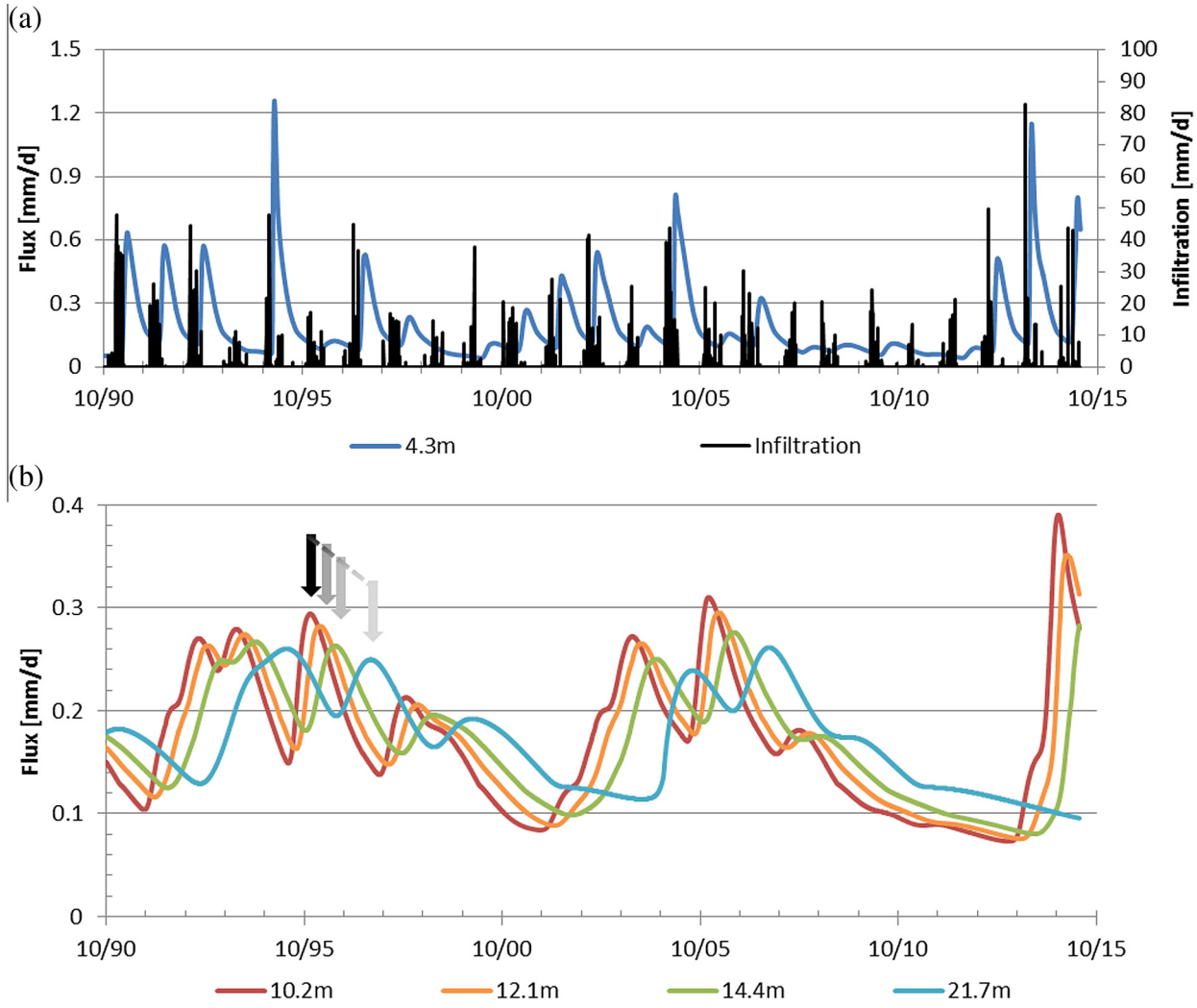

Fig. 9. Simulated surface infiltration (a), and vertical fluxes (a and b), at different depths for the bare soil scenario. The arrows indicate the flux peaks that are discussed in the text. (For interpretation of the references to color in this figure legend, the reader is referred to the web version of this article.)

Table 6
Simulated recharge for a 25-year period using mean estimated hydraulic conductivities and their ±10% variations (total mm, and % of precipitation).

	K_{s2} + 10%	K_{s2}	K_{s2} − 10%
K_{s1} + 10%	1574 mm, 29.5%	1567 mm, 29.4%	1559 mm, 29.3%
K_{s1}	1551 mm, 29.1%	1544 mm, 29.0%	1533 mm, 28.8%
K_{s1} − 10%	1533 mm, 28.6%	1517 mm, 28.5%	1508 mm, 28.3%

all scenarios, comparable to measurements and run-off estimates for loessial sediments (Yair, 1990; Givati and Atzmon, 2009; Eshtawi et al., 2015). The soil water content showed pronounced annual fluctuations, which were superimposed on smooth, multi-annual cycles. Soil water content, deep drainage, and recharge patterns are discussed in the following sections.

4.2.2. Bare soil

The initial water storage of 2076 mm (9.5% of pore volume) in the 22-m sediment profile of the bare soil scenario was the highest of all three scenarios. During winter periods, the upper part of the soil profile quickly gained moisture (up to 180 mm in some years), while during the following months it gradually dried. These changes can also be seen in the plots for the vertical fluxes (Fig. 9).

In the upper sandy layer (less than 4.3 m deep), large fluctuations in vertical fluxes can be observed closely resembling precipitation/infiltration events (Fig. 9a). Almost every annual cycle is comprised of an instantaneous rise in the flux followed by its gradual decrease. The flux usually starts to increase 40–60 days after the first major infiltration event. In some years, when infiltration is small, the rise in the flux is absent (e.g., 1993/94, 1998/99, 2010/11) or relatively small (e.g., 1995/96, 1999/2000, 2007/8, 2008/9). At the bottom of the sandy layer (4.3 m deep), due to surface evaporation and redistribution, the range of simulated fluxes is two orders of magnitude smaller than the range of surface infiltration fluxes.

Deeper in the sediment profile, the flux (and water content) fluctuations are much attenuated and tend to smooth out individual annual cycles. Individual flux peaks and dips at greater depths appear at larger time lags (Fig. 9b). For example, the peak that occurred at a depth of 4.3 m in January 1995 reached the depth of 10.2 m in Nov 1995, the depth of 12.1 m in Feb 1996, the depth of 12.4 m in July 1996, and the depth of 21.7 m in June 1997 (downward arrows in Fig. 9b). The vertical flux was correspondingly attenuated from 1.26 mm/d to 0.29 mm/d, 0.28 mm/d, 0.26 mm/d, and finally 0.25 mm/d at increasing depths, respectively. That reflects a time lag of about one year (November 1994–November 1995) at the bottom of the first clay horizon

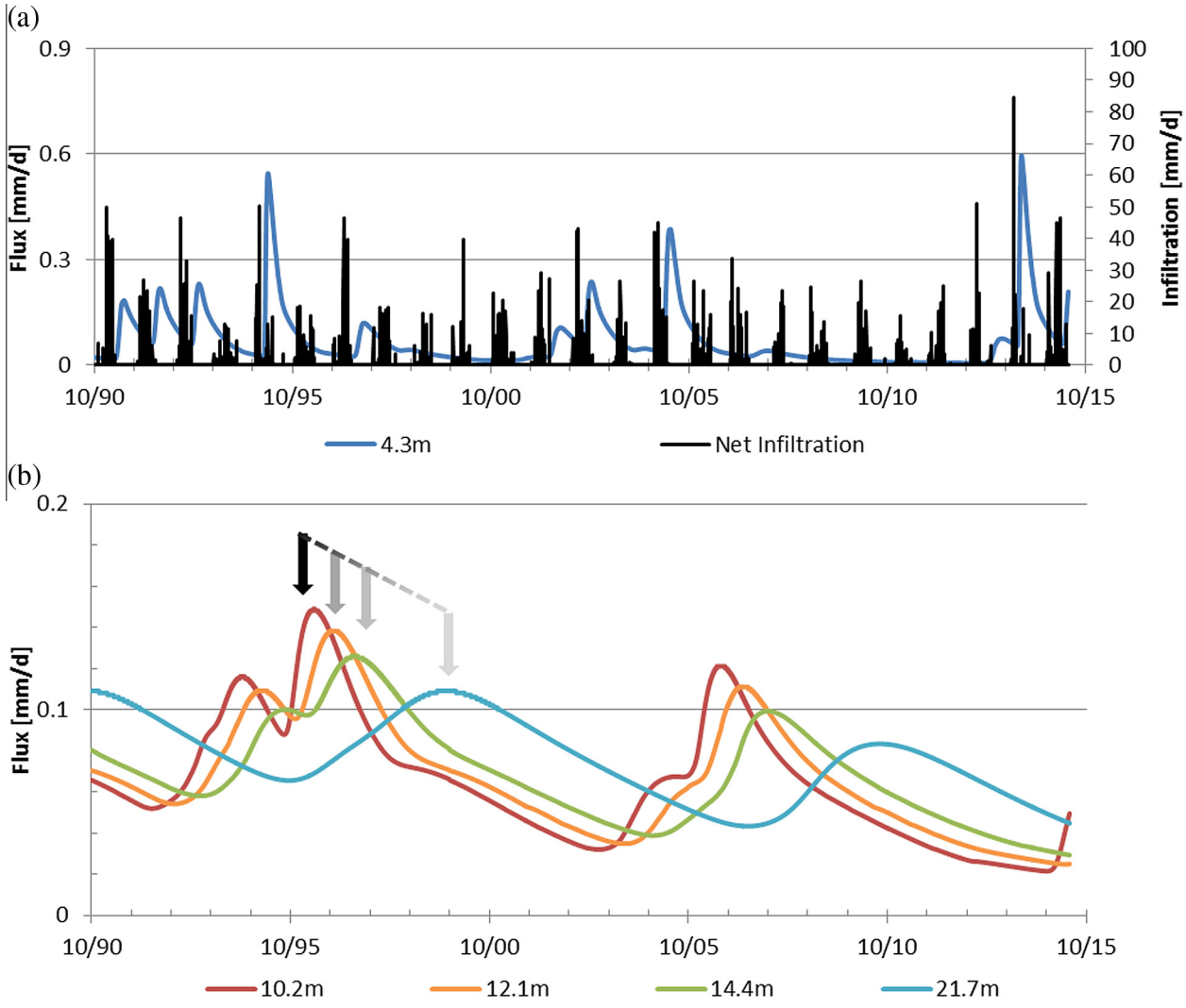

Fig. 10. Simulated surface infiltration (a), and vertical fluxes (a and b), at different depths for the semi-stabilized dunes scenario. The arrows indicate the flux peaks that are discussed in the text. (For interpretation of the references to color in this figure legend, the reader is referred to the web version of this article.)

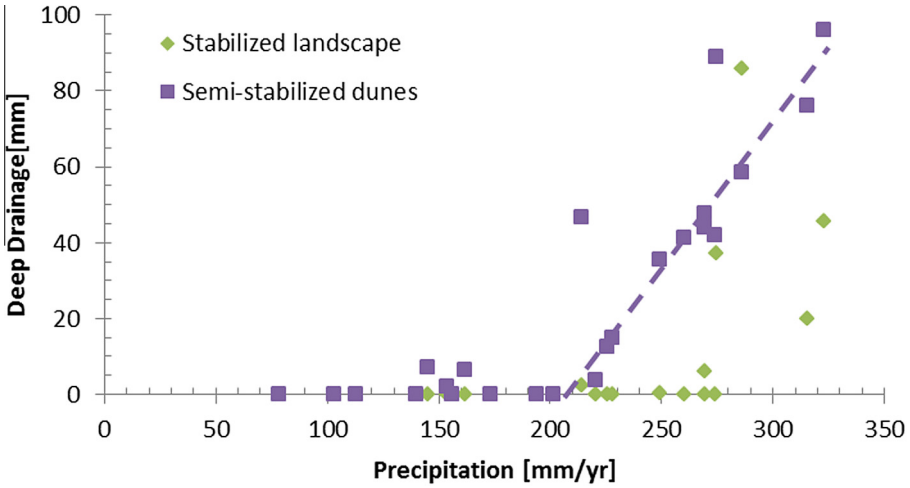

Fig. 11. Deep drainage vs. precipitation for the semi-stabilized and stabilized scenarios.

and up to a time lag of 2.5 years at the bottom of the 22-m sediment column. These trends (attenuations of annual signals and increasing time lags at deeper layers) are consistent with both theoretical considerations and field observations (e.g., Turkeltaub et al., 2015).

The overall recharge over the 25-year period is equivalent to 29% of the total precipitation. This value is very close to the range of estimated recharge rates for sandy loess soils (31–40%, Seiler and Gat, 2007). One should note that this is substantially less than recharge from sand dunes, which was lately reported to be about 72% of annual precipitation (Turkeltaub et al., 2015) and substantially more than an estimated range of recharge for silty loess soils (8–10%, Seiler and Gat, 2007).

Recharge rates were found to be relatively insensitive to small changes in hydraulic conductivities of the two soils. In further simulations, a ±10% change in soil hydraulic conductivities (K_{s1} *and* K_{s2}) resulted in a change of only ±2% in recharge (Table 6).

4.2.3. Semi-stabilized dunes

In the semi-stabilized dunes scenario, the initial water storage in the sediment profile, as well as the average water storage during the 25-year simulation, was 1901 mm. This value is about 8% lower than that for the bare soil scenario and reflects the effects of plant roots in removing water from the soil profile.

The fluctuations in the flux (and water content) resemble the pattern described for the bare soil scenario. However, the magnitude of fluxes is smaller, and their downward propagation is slower. For example, the peak of the winter 1995 flux is 0.57 mm/d for the semi-stabilized dunes scenario (Fig. 10a), while it is 1.25 mm/d for the bare soil scenario. The peak reached the depth of 10.2 m in April 1996, the depth of 12.1 m in November 1996, the depth of 14.2 m in May 1997, and the depth of 21.7 m in August 1999 (downward arrows in Fig. 10b). That corresponds to a time lag of about 1.5 years at the bottom of the first clay horizon and almost five years at the bottom of the 22-m sediment column.

It can be concluded that consideration of root water uptake in the upper 1 m of the soil profile reduced the overall soil water storage by about 8%, the peak flux by about 50%, and slowed the progress of the wetting front by about 50%. Additionally, the presence of plants reduced the overall recharge to 13% of total precipitation, with an average recharge of 28 mm/yr. In fact, during eight years there effectively was no deep drainage down from the root zone. During the other four years, only minimal (<20 mm/y) deep drainage occurred. As suggested in Fig. 11, a linear relationship may

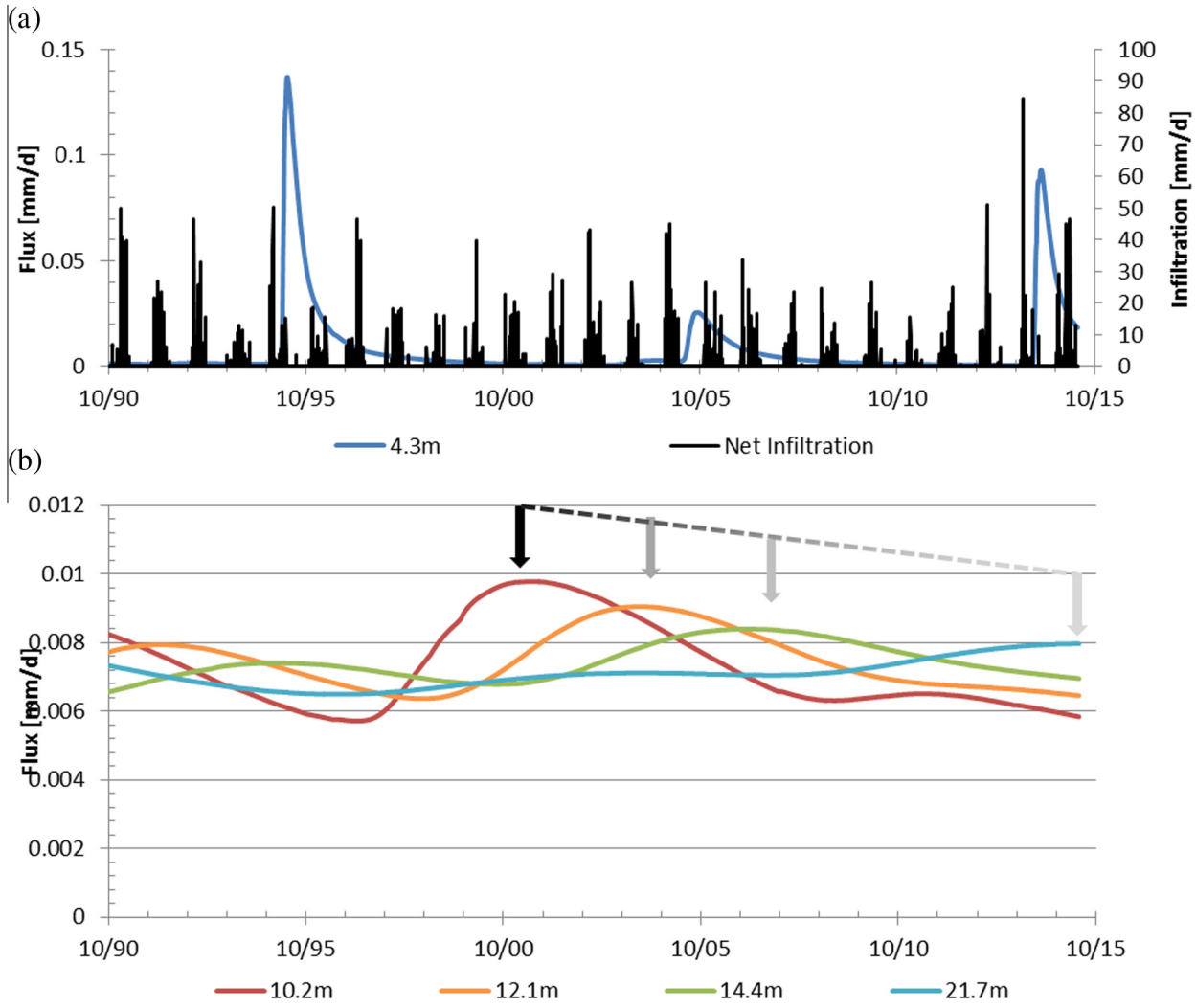

Fig. 12. Simulated surface infiltration (a), and vertical fluxes (a and b), at different depths for the stabilized landscape scenario. The arrows indicate the flux peaks that are discussed in the text. (For interpretation of the references to color in this figure legend, the reader is referred to the web version of this article.)

be interpreted between annual deep drainage and annual precipitation when the latter exceeds 210 mm/yr. In other words, for semi-stabilized loessial dunes, there is a threshold of 210 mm/yr before deep drainage occurs.

4.2.4. Stabilized landscape

For the stabilized landscape, the initial water storage in the sediment profile was 1544 mm, and the 25-year average was 1578 mm; both values are about 25% lower than for the bare soil scenario.

The effects of the vegetation (roots) on the amplitude and temporal fluctuations in the flux (and water contents) discussed above increased for this scenario, with roots extending down to a depth of 3 m. The infiltration peak of winter 1994/1995 reached the depth of 4.3 m in April 1995 (6 months after the first major infiltration event) with a peak of 0.14 mm/d (Fig. 12a). It reached the depth of 10.2 m in April 2001, with a flux of 0.0097 mm/d, and the depth of 21.7 m at the end of the simulation, with a flux of 0.008 mm/d (downward arrows in Fig. 12b). That reflects a time lag of about 6.5 years at the bottom of the first clay horizon and more than 20 years at the bottom of the 22-m sediment column.

It can be concluded that consideration of plant roots in the upper 3 m of the soil profile reduced the overall soil water storage by about 26%, the water flux peaks by 88–96%, and slowed the progress of the wetting fronts by a factor of 5–7. Overall recharge was reduced in this scenario to only about 1% of total precipitation, with an average annual recharge of 2.5 mm/yr. In fact, during most years, there effectively was no deep drainage down from the root zone. During only four years was the deep drainage substantial (>20 mm). When annual deep drainage is plotted against annual precipitations, it appears that deep drainage occurs only when precipitation is higher than 270 mm/y, yet its magnitude is unpredictable (Fig. 11).

4.3. Discussion

The following section utilizes the simulated results to discuss two prominent issues: (a) the relationship between annual precipitation and recharge, and (b) the effect of vegetation on the overall recharge rates. These two factors have an important impact on our ability to predict recharge from precipitation and its representation in numerical models.

4.3.1. Recharge–precipitation relationship

As noted before and demonstrated in Fig. 13a, there is no clear correlation between annual recharge in loessial sediments and annual precipitation for any of the evaluated scenarios. Also, there is no correlation between annual recharge and annual precipitation of the preceding year. These two correlations have been successfully tested to predict recharge for non-vegetated sandy soil profiles (Turkeltaub et al., 2015). There is no strong linear correlation even between annual precipitation and annual recharge shifted by 2.5, 5, and 20 years (Fig. 13b), reflecting the propagation of the moisture front in the three evaluated scenarios, respectively.

These results are not surprising and demonstrate the importance of the capacity of the soil profile in buffering short-term fluxes (i.e., rain events). On average, only 7.0–9.5% of the pore volume is filled with water, allowing substantial fluctuations in the water storage to occur. This buffering capacity is strengthened by the layered structure of the sediment profile. In the studied case, vertical flow is accompanied by water movement from sandy clay loam horizons with water contents of 13–15% to sandy loam horizons with water contents of 6–8% and back. That is, recharge, contrary to net infiltration, cannot be predicted on the basis of annual

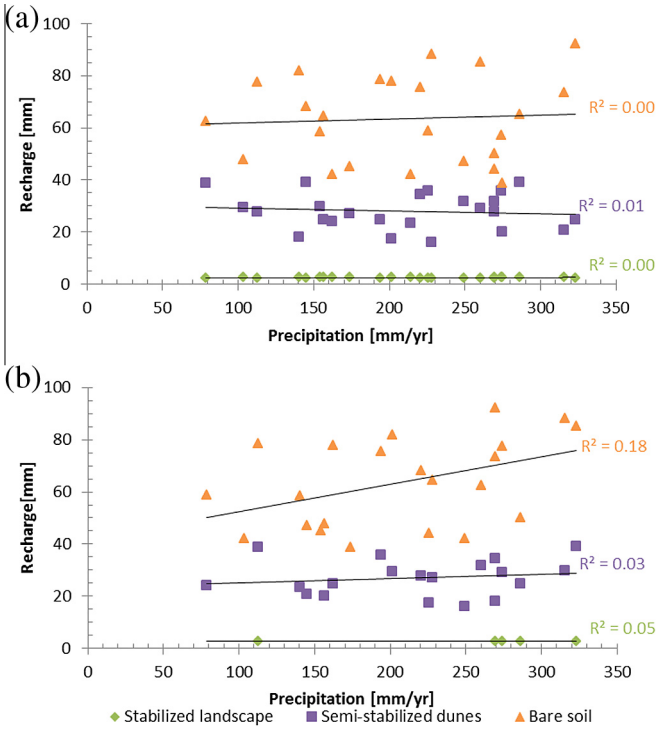

Fig. 13. Annual recharge vs. annual precipitation (a) of the same year and (b) shifted according to the wetting front propagation, i.e., +2 yr for bare soil, +5 yr for semi-stabilized dunes, and +20 yr for the stabilized landscape. Linear trend lines and R2 are shown for each scenario.

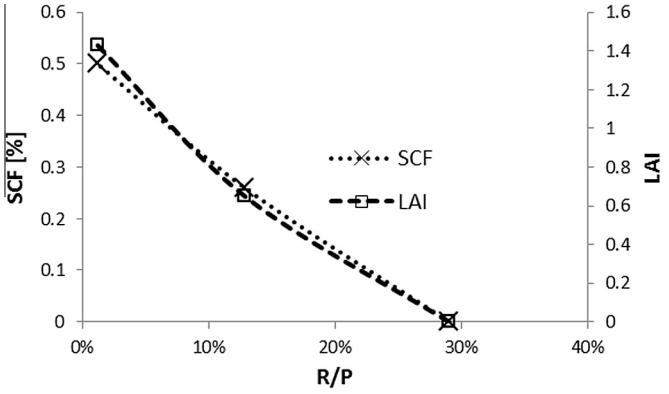

Fig. 14. Overall simulated recharge (as %*R*/*P*) as a function of SCF and LAI.

precipitation, as the soil acts as a multi-annual storage to 'buffer' infiltration.

In agreement with previous studies (e.g., Wu et al., 1996), this research demonstrates that recharge estimations, as a constant fraction of annual precipitation, may be an over-simplified approach. Rather, dynamic models that account for the soil capacity to buffer water fluxes (e.g., Wu et al., 1997; Sheffer et al., 2010) need to be used.

4.3.2. Effects of dune stabilization and natural vegetation on recharge

Similar to the recent literature (e.g., Hugenholtz and Koenig, 2014; Bar Kutiel et al., 2016), the results of this study suggest that dune stabilization, through the establishment of local vegetation, reduces the water content in the sediment profile and subsequently the groundwater recharge. Bare sandy loess may serve as an important source of recharge and may provide long-term

Table 7
Calculated travel time for matrix flow in the loessial sediments.

	Mean recharge [mm/yr]	Volume of water in the soil profile [mm]	Travel time to 22 m depth [yr]	Interpolated travel time to 30 m depth [yr]
Bare soil	63.5	2076	33	45
Semi-stabilized dunes	28.0	1901	68	92
Stabilized landscape	2.6	1544	>500	808

recharge of up to 30% of precipitation. Semi-stabilized dunes with scattered vegetation and a limited root depth of up to 1 m reduce recharge rates by nearly half, whereas stabilized loess landscapes with mature vegetation may prevent recharge altogether or allow only minimal recharge of about 1% of precipitation. Simulation results show that an increase in SCF and/or LAI results in a (nearly linear) reduction of recharge as a fraction of precipitation (R/P) (Fig. 14). This trend has many physical and biological reasons, the main one being the presence of the rooting zone and thus the greater ability to capture infiltrated water and return it to the atmosphere in the form of transpiration (Kurtzman and Scanlon, 2011). In other words, while recharge may not be accurately predicted on an annual basis, the long-term R/P can be determined solely from the vegetation coverage factors (LAI or SCF).

4.3.3. Travel time

As a by-product of the recharge simulations, one can calculate the travel time of water from the soil surface to the groundwater table. A travel time of 33 years to a depth of 22 m can be calculated for the bare soil scenario assuming a 'piston flow' through the soil matrix, a recharge rate of 63.5 mm/yr, and water storage of 2076 mm. Interpreting this value for a water table depth of 30 m would result in a travel time of 45 years. Corresponding values for the semi-stabilized dunes and stabilized landscape scenarios would produce travel times of 92 years and more than 800 years, respectively (Table 7). This time range is aligned with findings of other arid zones loess recharge studies (Huang et al., 2013)

5. Summary

The transient nature of recharge through layered loessial sediments at the edge of arid zones was investigated using a Richards' equation-based model. First, the sediment profile was conceptualized, and then the van Genuchten parameters of the soil hydraulic properties were quantified using the dataset collected during the large infiltration test by Gvirtzman et al. (2008) and the inverse method in the HYDRUS-2D numerical code. Simulation results and the grain-size distribution classified the two soils, which formed different horizons of the sediment profile, as sandy loam and sandy clay loam. The calibrated saturated hydraulic conductivities of these two soils were found to be lower than previously reported, with an average hydraulic conductivity of 80.2 cm/d for the sandy loam and 17.3 cm/d for the sandy clay loam.

Next, diffuse recharge originating from natural precipitation over layered loessial sediments was investigated using HYDRUS-1D for three geomorphological conditions of bare soils, semi-vegetated dunes, and a stabilized landscape. The buffering effect of the layered sediment profile attenuated the vertical fluxes and masked the signal of individual years, resulting in a multi-annual recharge pattern. Thus, it is no surprise that no correlation was found between annual recharge and annual precipitation. On the contrary, groundwater recharge occurs year-round with relatively small multi-annual changes. This research demonstrates, in agreement with related literature, that recharge estimations as a constant fraction of annual precipitation may be an over-simplified approach.

The HYDRUS simulations also show that vegetation maturity is an important factor in determining the long-term recharge capacity of porous sediments. In general, recharge rates decrease with an increase in the vegetation cover. For the evaluated layered sandy loess, the recharge rate decreased from nearly 30% for bare soils to only about 1% of precipitation under stabilized landscapes having a 50% vegetation cover.

These findings suggest that the long-term recharge (as R/P) can be determined by accounting for the vegetation cover. Dynamic models, which can account for the soil capacity to buffer water fluxes (e.g., this study; Sheffer et al., 2010), should still be used to estimate recharge time series.

Acknowledgements

The authors thank Dr. Onn crouvi (Geological Survey of Israel) for valuable input regarding the loess origin, and Talia Hurowitz (IMS) for clarification of the meteorological data inventory. The manuscript was improved following comments of three anonymous reviewers.

References

Aish, A.M., 2014. Estimation of water balance components in the Gaza Strip with GIS based WetSpass model. Civ. Environ. Res. 6 (11), 77–84.
Amir, N., Kafri, U., Herut, B., Shalev, E., 2013. Numerical simulation of submarine groundwater flow in the coastal aquifer at the Palmahim area, the Mediterranean coast of Israel. Water Resour. Manage. 27 (11), 4005–4020. http://dx.doi.org/10.1007/s11269-013-0392-2.
Bar Kutiel, P., Katz, O., Ziso-Cohen, V., Divinsky, I., Katra, I., 2016. Water availability in sand dunes and its implications for the distribution of Artemisia monosperma. Catena 137, 144–151. http://dx.doi.org/10.1016/j.catena.2015.09.007.
Crouvi, O., Amit, R., Enzel, Y., Gillespie, A.R., 2010. Active sand seas and the formation of desert loess. Quatern. Sci. Rev. 29 (17–18), 2087–2098. http://dx.doi.org/10.1016/j.quascirev.2010.04.026.
Eshtawi, T., Evers, M., Tischbein, B., 2015. Quantifying the impact of urban area expansion on groundwater recharge and surface runoff. Hydrol. Sci. J. http://dx.doi.org/10.1080/02626667.2014.1000916.
Feddes, R.A., Kowalik, P.J., Zaradny, H., 1978. Simulation of Field Water Use and Crop Yield. John Wiley & Sons, New York.
Fetter, C.W., 2001. Applied Hydrogeology, fourth ed. Prentice-Hall, New Jersey.
Givati, A., Atzmon, B., 2009. Model to predict flood-flow volume in the catchments: Yarqon, Soreq, Lakhish, and Besor. Rep. Hydro/2009/01. Israeli Hydrological Service (IHS), Jerusalem, 28 pp (Hebrew).
Gvirtzman, H., Shalev, E., Dahan, O., Hatzor, Y.H., 2008. Large-scale infiltration experiments into unsaturated stratified loess sediments: monitoring and modeling. J. Hydrol. 349, 214–229.
Hatzor, Y.H., Gvirtzman, H., Wainshtein, I., Orian, I., 2009. Induced liquefaction experiment in relatively dense, clay-rich sand deposits. J. Geophys. Res. 114, B02311. http://dx.doi.org/10.1029/2008JB005943.
Helsel, D.R., Hirsch, R.M., 2002. Statistical methods in water resources. In: Techniques of Water-Resources Investigations of the United States Geological Survey – Book 4, Hydrologic Analysis and Interpretation. USGS.
Hillel, D., 2004. Introduction to Environmental Soil Physics. Elsevier Academic Press, Amsterdam.
Hopmans, J.W., Šimůnek, J., Romano, N., Durner, W., 2002. Inverse modeling of transient water flow. In: Dane, J.H., Topp, G.C. (Eds.), Methods of Soil Analysis – Part 4, Physical Methods, third ed. SSSA, Madison, WI, pp. 963–1008.
Huang, T., Pang, Z., Edmunds, W.M., 2013. Soil profile evolution following land-use change: implications for groundwater quantity and quality. Hydrol. Process. 27 (8), 1238–1252. http://dx.doi.org/10.1002/hyp.9302.
Hugenholtz, C.H., Koenig, D.K., 2014. Sand dune stabilization reduces infiltration and soil moisture: a case study from the northern Great Plains. Ecohydrology 7 (4), 1135–1146. http://dx.doi.org/10.1002/eco.1445.
Jacques, D., Šimůnek, J., Timmerman, A., Feyen, J., 2002. Calibration of Richards' and convective–dispersion equations to field-scale water flow and solute transport

under rainfall conditions. J. Hydrol. 259, 15–31. http://dx.doi.org/10.1016/S0022-1694(01)00591-1.
Kurtzman, D., Scanlon, B.R., 2011. Groundwater recharge through vertisols: irrigated cropland vs. natural land, Israel. Vadose Zone J. 10, 662–674.
Leterme, B., Mallants, D., Jacques, D., 2012. Sensitivity of groundwater recharge using climatic analogues and HYDRUS-1D. Hydrol. Earth Syst. Sci. 16 (8), 2485–2497. http://dx.doi.org/10.5194/hess-16-2485-2012.
Lin, R., Wei, K., 2006. Tritium profiles of pore water in the Chinese loess unsaturated zone: implications for estimation of groundwater recharge. J. Hydrol.
Marquardt, D.W., 1963. An algorithm for least-squares estimation of nonlinear parameters. J. Soc. Ind. Appl. Math. 11 (1), 431–441. http://dx.doi.org/10.1137/0111030.
Mualem, Y., 1976. A new model for predicting the hydraulic conductivity of unsaturated porous media. Water Resour. Res. 12 (3), 513–522.
Petersen, C.T., Trautner, A., Hansen, S., 2008. Spatio-temporal variation of anisotropy of saturated hydraulic conductivity in a tilled sandy loam soil. Soil Tillage Res. 100 (1–2), 108–113. http://dx.doi.org/10.1016/j.still.2008.05.004.
Radcliffe, D.E., Šimůnek, J., 2010. Soil Physics with HYDRUS – Modeling and Applications. CRC Press, 373 pp.
Radcliffe, J.C., 2002. Pesticide Use in Australia. Australian Academy of Technological Sciences and Engineering, Parkville, Victoria, 310 pp.
Ritchie, J.T., 1972. Model for predicting evaporation from a row crop with incomplete cover. Water Resour. Res. 8 (5), 1204–1213.
Ritter, A., Hupet, F., Muñoz-Carpena, R., Lambot, S., Van-clooster, M., 2003. Using inverse methods for estimating soil hydraulic properties from field data as an alternative to direct methods. Agric. Water Manage. 59, 77–96.
Scanlon, B., Healy, R., Cook, P., 2002a. Choosing appropriate techniques for quantifying groundwater recharge. Hydrogeol. J. 10 (1), 18–39. http://dx.doi.org/10.1007/s10040-001-0176-2.
Scanlon, B.R., Christman, M., Reedy, R.C., Porro, I., Šimůnek, J., Flerchinger, G.F., 2002b. Intercode comparisons for simulating water balance of surficial sediments in semiarid regions. Water Resour. Res. 38 (12), 1323. http://dx.doi.org/10.1029/2001WR001233.
Scanlon, B.R., Keese, K.E., Flint, A.L., Flint, L.E., Gaye, C.B., Edmunds, W.M., Simmers, I., 2006. Global synthesis of groundwater recharge in semiarid and arid regions. Hydrol. Process. 20, 3335–3370.
Seiler, K.P., Gat, J.R., 2007. Groundwater Recharge from Run-off, Infiltration and Percolation. Springer.
Sheffer, N., Dafny, E., Gvirtzman, H., Navon, S., Frumkin, A., Morin, E., 2010. Hydrometeorological daily recharge assessment model (DREAM) for the Western Mountain Aquifer, Israel: model application and effects of temporal patterns. Water Resour. Res. 46, W05510. http://dx.doi.org/10.1029/2008WR007607.
Šimůnek, J., van Genuchten, M.T., Šejna, M., 2008. Development and applications of the HYDRUS and STANMOD software packages and related codes. Vadose Zone J. 7 (2), 587–600. http://dx.doi.org/10.2136/VZJ2007.0077.
Šimůnek, J., Šejna, M., Saito, H., Sakai, M., van Genuchten, M.T., 2009. The HYDRUS-1D Software Package for Simulating the One-dimensional Movement of Water, Heat, and Multiple Solutes in Variably-saturated Media Version 4.08. Dep. of Environ. Sci., Univ. of California, Riverside.
Tulmatz, Y., 1977. Hydrogeological Atlas of Israel – The Coastal Basin. The Hydrological Service, Israel Water Authority, Jerusalem.
Turkeltaub, T., Kurtzman, D., Bel, G., Dahan, O., 2015. Examination of groundwater recharge with a calibrated/validated flow model of the deep vadose zone. J. Hydrol. 522, 618–627. http://dx.doi.org/10.1016/j.jhydrol.2015.01.026.
van Genuchten, M.T., 1980. A closed-form equation for predicting the hydraulic conductivity of unsaturated soils. Soil Sci. Soc. Am. J. 44 (5), 892–898.
Vrugt, J.A., Stauffer, P.H., Wöhling, T., Robinson, B.A., Vesselinov, V.V., 2008. Inverse modeling of subsurface flow and transport properties: a review with new developments. Vadose Zone J. 7 (2), 843–864.
Wang, W., Neuman, S.P., Yao, T., Wierenga, P.J., 2003. Simulation of large-scale field infiltration experiments using a hierarchy of models based on public, generic and site data. Vadose Zone J. 2, 297–312.
Weinthal, E., Vengosh, A., Marei, A., Gutierrez, A., Kloppmann, W., 2005. The water crisis in the Gaza Strip: prospects for resolution. Ground Water 43 (5), 653–660.
Wesseling, J.G., Elbers, J.A., Kabat, P., van den Broek, B.J., 1991. SWATRE: Instructions for Input (Internal Notes). Winand Staring Centre, Wageningen, The Netherlands.
Wierenga, P.J., Hills, R.G., Hudson, D.B., 1991. The Las Cruces trench site: characterization, experimental results, and one-dimensional flow predictions. Water Resour. Res. 27 (10), 2695–2705.
Wu, J., Zhang, R., Yang, J., 1996. Analysis of rainfall-recharge relationships. J. Hydrol. 177 (1–2), 143–160. http://dx.doi.org/10.1016/0022-1694(95)02935-4.
Wu, J., Zhang, R., Yang, J., 1997. Estimating infiltration recharge using a response function model. J. Hydrol. 198 (1–4), 124–139. http://dx.doi.org/10.1016/S0022-1694(96)03309-4.
Yaalon, D.H., Dan, J., 1974. Accumulation and distribution of loess-derived deposits in the semi-desert and desert fringe areas of Israel. Zeitschrift fur Geomorphologie Supplementband 20, 91–105.
Yair, A., 1990. The role of topography and surface cover upon soil formation along hillslopes in arid climates. Geomorphology 3, 287–299.
Zou, Z.Y., Young, M.H., Li, Z., Wierenga, P.J., 2001. Estimation of depth averaged unsaturated soil hydraulic properties from infiltration experiments. J. Hydrol. 242 (1–2), 26–42. http://dx.doi.org/10.1016/S0022-1694(00)00385-1.